Journal of Alloys and Compounds 509 (2011) 9399–9405

Contents lists available at ScienceDirect

Journal of Alloys and Compounds

journal homepage: www.elsevier.com/locate/jallcom

Overlapping large polaron tunneling conductivity and giant dielectric constant in $Ni_{0.5}Zn_{0.5}Fe_{1.5}Cr_{0.5}O_4$ nanoparticles (NPs)

Muhammed Tan[a], Yüksel Köseoğlu[a,*], Furkan Alan[a], Erdoğan Şentürk[b]

[a] Department of Physics, Fatih University, Istanbul 34500, Turkey
[b] Department of Physics, Sakarya University, Sakarya 54100, Turkey

ARTICLE INFO

Article history:
Received 17 June 2011
Received in revised form 19 July 2011
Accepted 21 July 2011
Available online 27 July 2011

Keywords:
Spinel Ni–Zn ferrite
High dielectric constant
Diffuse phase transition
Overlapping large polaron tunneling

ABSTRACT

We report an orderly study on the structural and dielectric properties of $Ni_{0.5}Zn_{0.5}Cr_{0.5}Fe_{1.5}O_4$ nanoparticles (NPs) synthesized by a polyethylene glycol (PEG)-assisted hydrothermal technique. XRD, FT-IR, FE-SEM and EDX measurements were implemented for the structural, morphological and compositional investigations of the product. Dielectric spectroscopy was used for the dielectric property investigation of the sample. Average particle size of the nanoparticles was estimated using Debye–Scherrer's equation as 34 nm. Electrical properties of the sample have been investigated in the range of 1 Hz to 3 MHz (233–412 K). It is observed that the sample has a giant dielectric constant approaching to 10^6 within the examined temperature range. It is also determined that the sample exhibits a dispersive phase transition around 305 K at which this giant value of dielectric constant has been obtained. This transition has been characterized by Diffuse Phase Transition. Temperature and frequency dependence of dielectric loss function has been attributed to surface charges for the short-time relaxations and to hopping electrons for the long-time relaxations. At low frequencies, dielectric loss function has been supported by the modified Cole–Cole equation. Frequency and temperature dependent conductivity behavior of the sample has been explained by Overlapping Large Polaron Tunneling model.

1. Introduction

There is a growing interest on mixed nanoferrite systems in the last decades due to their remarkable physical, chemical and structural properties owing to their extremely small size, large specific area and a number of promising applications. The spinel ferrites belong to an important group of magnetic materials, because of their significant magnetic properties particularly in radio frequency region, physical flexibility, high electrical resistivity, mechanical hardness and chemical stability [1–4]. For their excellent properties more attention was paid on mixed spinel ferrites, which are mainly applied in electrical devices and in catalysis.

A complete sort of distribution of cations is possible in ferrites, whose crystal chemical formula can be generally represented by $(M^{2+}_{1-\lambda}Fe^{3+}_{\lambda})[M^{2+}_{\lambda}Fe^{3+}_{2-\lambda}]O_4$ where parentheses and square brackets denote cation sites of tetrahedral (A) and octahedral [B] coordination, respectively [5]. The term λ represents the so-called degree of inversion defined as the fraction of the (A) sites occupied by Fe^{3+} cations. The cation arrangement can vary between two extreme cases. One of them is the normal spinel ($\lambda = 0$), where all the divalent M cations occupy (A) sites and all the trivalent Fe cations occupy [B] sites. The other one is the inverse spinel ($\lambda = 1$), where all the divalent ions occupy [B] sites and trivalent cations are equally distributed between (A) and [B] sites. Spinels with the cation distribution intermediate between normal and inverse (i.e., partially inverse spinels; $0 < \lambda < 1$) are also very frequent. The properties of spinel ferrites are highly responsive to the cation distribution which in turn depends on the technique of preparation [6].

Ni–Zn ferrite is a kind of soft magnetic material with low coercivity that is both to gain and lose magnetization [7–10]. Nickel–zinc ferrites have vast applications in both low and high frequency devices. They play an important role in many technological applications because of their high resistivity, low dielectric loss, mechanical hardness, high Curie temperature and chemical stability [11,12]. The dielectric behavior gives sufficient information about localized electric charge carries, leading to a greater understanding of mechanism of dielectric polarization in the ferrite system [13]. The dielectric property is one of the properties of the ferrites, which depends on the method of preparation, sintering time, sintering condition, chemical composition, type and amount of additives [13]. Several researchers have studied dielectric properties of Ni–Zn ferrites prepared by ceramic method [13–17]. Enhanced permeability and dielectric constant of Ni–Zn ferrite synthesized in nanocrystalline form by a combustion method has been studied by Deka and Joy [18]. They have found very high initial permeability at 1 MHz with low loss and very high dielectric

* Corresponding author. Tel.: +90 212 8663300x2049; fax: +90 212 8890832.
E-mail address: yukselk@fatih.edu.tr (Y. Köseoğlu).

0925-8388/$ – see front matter © 2011 Elsevier B.V. All rights reserved.
doi:10.1016/j.jallcom.2011.07.063

constant at lower frequencies as compared to ceramic method. They also reported that electrical properties like resistivity and dielectric constant depend on sintering time. Ajmal and Maqsood [17] have studied AC conductivity, density related and magnetic properties of $Ni_{1-x}Zn_xFe_2O_4$ ferrites with the variation of zinc concentration. They reported that AC conductivity (σ_{ac}) increases with increase in zinc concentration at the frequency of 1 kHz.

Structural and electromagnetic properties of Ni–Zn ferrites prepared by sol–gel combustion method have been studied by Azadmanjiri [19]. He reported that dielectric constant, dielectric loss and complex dielectric constant were influenced by zinc concentration. Gul et al. [20] studied electrical and magnetic characterization of nanocrystalline Ni–Zn ferrite synthesized by co-precipitation route. They stated that dielectric constant follows the Maxwell–Wagner interfacial polarization. The dielectric behavior of the Ni–Zn ferrites as a function of frequency, sintering temperature and sintering time was reported by Rao and Rao [21]. Furthermore, Sheikh and Mathe [22] have studied anomalous electrical properties of nanocrystalline Ni–Zn ferrites. They found less dielectric loss for the samples sintered at 900 °C compared to that sintered at 400 °C.

In this article, we report the electrical behavior of a specific composition of Cr (III) substituted Ni–Zn ferrite NPs prepared by polyethylene glycol (PEG) assisted hydrothermal technique.

2. Experimental

2.1. Synthesis

For the suitable chemical reaction to take place, stoichiometric molar amounts of hydrous nickel chloride [$NiCl_2{\cdot}6H_2O$] (0.004 mol), chromium (III) oxide [Cr_2O_3] (0.002 mol) and zinc chloride [$ZnCl_2$] (0.004 mol) were each dissolved in beakers filled with 7 mL of de-ionized water. Likewise, 0.012 mol of hydrous ferric chloride [$FeCl_3{\cdot}6H_2O$] was dissolved in 10 mL of de-ionized water. Then all of the solutions were stirred with the aid of a magnetic stirrer, and after that, the solutions were mixed and stirred altogether once more for 10 min. During the last stirring, 10 mL of PEG-400 was poured into the solution to serve as a surfactant to cover NPs and prevent agglomeration. Then 32% NaOH solution was also added to the solution drop by drop to make the medium basic. The hydroxyl ions rendered formation of NPs possible. Then with a little more NaOH addition, the pH of the solution was adjusted to 11.5. The obtained solution was put into an autoclave (50 mL) up to two thirds of its volume. Lastly, the autoclave was left in an oven at 180 °C for 24 h.

After cleaning the sample a few times by using a centrifuge machine with de-ionized water and absolute ethanol, the sample was again put in an oven at 70 °C to dry. Taken solid phase sample was grinded in a mortar to make it powder. Obtained powder was used for all of the measurements. For SEM and electrical property investigations, the powder was pressed as circular plate.

2.2. Measurements

- X-ray powder diffraction analysis was conducted on a Huber JSO-DEBYEFLEX 1001 Diffractometer (XRD) using CuK_α (operated at 40 kV and 35 mA).
- FT-IR transmission spectra were taken on Mattson Satellite Infrared Spectrometer from 4000 to 400 cm^{-1}.
- Field Emission Scanning Electron Microscope (FE-SEM, JEOL 7001 FE with EDX) was used in order to investigate the nanostructure, morphology and elemental composition of the sample. Sample was coated with carbon prior to SEM analysis.
- Conductivity (ac–dc) measurements of the product were studied by Novocontrol dielectric spectroscopy in the range 233–413 K with a step of 20 K (frequency range 1 Hz to 3 MHz).

3. Results and discussion

3.1. XRD analysis

Fig. 1 represents the XRD pattern of $Ni_{0.5}Zn_{0.5}Cr_{0.5}Fe_{1.5}O_4$ NPs. X-ray diffraction study of the sample that confirmed the formation of single phase cubic spinel structure, without any impurity phases. The average crystallite diameter D_{XRD}, was estimated by the Debye–Scherrer equation $D = 0.9\lambda/\beta\cos\theta_B$ {where D is the crystallite size, λ is the wavelength of CuK_α, β is the full width at half maximum (FWHM) of the most dense diffraction peak, and θ_B is the Bragg's angle} [14,15]. The result shows that the particle size of $Ni_{0.5}Zn_{0.5}Cr_{0.5}Fe_{1.5}O_4$ sample is around 34 nm.

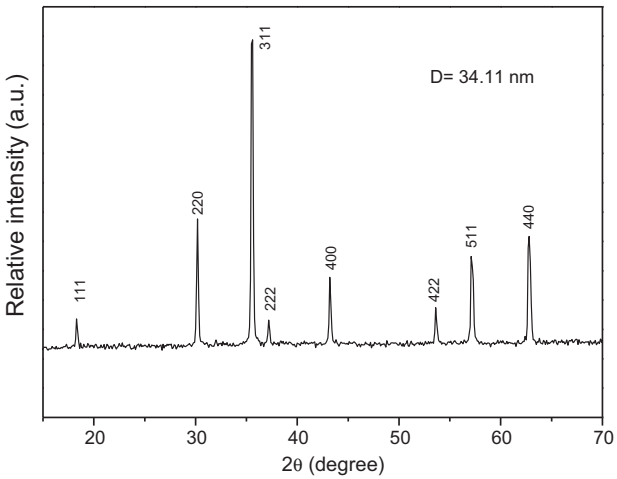

Fig. 1. XRD patterns of $Ni_{0.5}Zn_{0.5}Cr_{0.5}Fe_{1.5}O_4$, nanoparticles, synthesized by PEG-assisted hydrothermal technique.

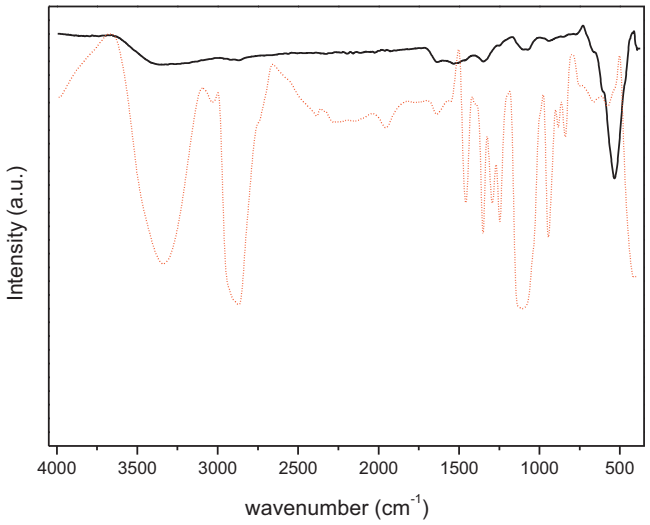

Fig. 2. FT-IR spectra of $Ni_{0.5}Zn_{0.5}Cr_{0.5}Fe_{1.5}O_4$ nanoparticles and PEG (dashed red line).

3.2. FT-IR spectroscopy

Two main broad metal-oxygen bands are seen in the IR spectra of all spinels, and ferrites in particular. The highest one, ν_1, (Fig. 2) usually observed in the range 600–550 cm^{-1} corresponds to intrinsic stretching vibrations of the metal at the tetrahedral site, $M_{tetra} \leftrightarrow O$, whereas the ν_2-lowest band, typically observed in the range 450–385 cm^{-1}, is assigned to octahedral-metal stretching, $M_{octa} \leftrightarrow O$ [16,17]. It is known that Ni^{2+} and Cr^{3+} ions have octahedral-site preference, whereas in a normal-spinel $ZnFe_2O_4$, Zn^{2+} prefers the tetrahedral site [23,24]. Fe^{3+} ions can occupy both octahedral and tetrahedral sites [18]. However, no clear peak due to metal ions at the octahedral site has been observed which is predictable to occur below 400 cm^{-1}. This may be due to the broadening of this peak attributed to very tiny particles of spinel ferrites [19].

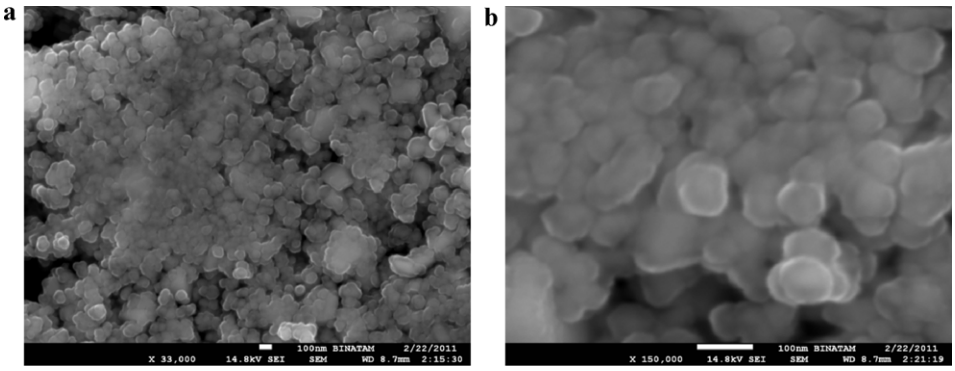

Fig. 3. SEM micro-graphs of $Ni_{0.5}Zn_{0.5}Cr_{0.5}Fe_{1.5}O_4$ nanoparticles.

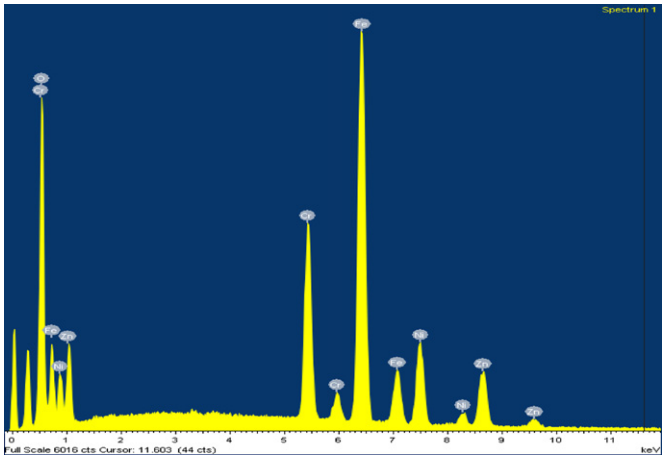

Fig. 4. EDX spectrum for $Ni_{0.5}Zn_{0.5}Cr_{0.5}Fe_{1.5}O_4$ nanoparticles.

3.3. Scanning electron microscopy

Fig. 3(a and b) depicts field emission scanning electron micrographs (FE-SEM) of $Ni_{0.5}Zn_{0.5}Cr_{0.5}Fe_{1.5}O_4$ NPs taken at two different magnifications. SEM images reveal that the sample consists of regular shaped spherical NPs with the presence of soft agglomeration. A close view of particles also reveals that smaller crystallites have sizes less than 100 nm. Nanoparticles were dense and distributed evenly on the whole mass. In addition to this, although these smaller crystallites are so closely arranged together, a clear boundary between neighboring crystallites can still be observed (Fig. 3(b)).

3.4. Energy dispersion X-ray analysis

The elemental composition of synthesized $Ni_{0.5}Zn_{0.5}Cr_{0.5}Fe_{1.5}O_4$ NPs has been investigated by the energy dispersion X-ray (EDX) analysis. Fig. 4 shows EDX patterns of the $Ni_{0.5}Zn_{0.5}Cr_{0.5}Fe_{1.5}O_4$ NPs. From the EDX spectrum, the presence of Zn, Ni, Fe, Cr and O has been confirmed and calculated percentages reveal almost the same ratio of Zn/Ni/Fe/Cr for the synthesized NPs as they were actually added during synthesis process (see Table 1).

Table 1
The mass ratios of elements as ideally expected from the chemical formula $Ni_{0.5}Zn_{0.5}Cr_{0.5}Fe_{1.5}O_4$ and as obtained from the EDX measurement.

Mass ratios	Ni (%)	Zn (%)	Fe (%)	Cr (%)	O (%)	Total (%)
As expected	12.44	13.86	35.54	11.03	27.13	100.00
EDX results	12.32	13.67	37.56	12.42	24.03	100.00

3.5. Dielectric studies

3.5.1. Real part of dielectric constant

Temperature and frequency variance of the system of $Ni_{0.5}Zn_{0.5}Cr_{0.5}Fe_{1.5}O_4$ NPs is shown in Fig. 5 where an anomaly widely dispersed around the temperature of 305 K can be seen.

Temperature variance of dielectric constant, broadening of the peak along a wide temperature range, deflection from Curie–Weiss law around the phase transition temperature and the presence of frequency dispersion in dielectric constant and the tangent loss support the phenomena of diffuse phase transition (DPT) [25]. According to DPT, the temperature variance of dielectric constant is expressed as

$$\frac{1}{\varepsilon(w,T)} = \frac{1}{\varepsilon_m(w,T)} + \frac{[T - T_m(w)]^{\gamma}}{2\varepsilon_m(w,T)\delta^2} \quad (1)$$

Here, ε_m is the maximum value of dielectric constant, T_m is the temperature at which this value has been measured, γ is the diffuseness parameter and δ is a constant. The parameter γ is generally in the range of $1 < \gamma < 2$ and gives information about characteristics of phase transition. The parameter γ takes the value of 1 for ferroelectric samples abiding by Curie–Weiss law and equals to 2 for completely disordered systems. This parameter can easily be estimated from the linear slope of $\ln(1/\varepsilon - 1/\varepsilon_m)$ vs. $\ln(T - T_m)$. The values of γ and δ obtained by fitting the experimental results of 10 kHz measurements with Eq. (1) are 1.85 and 21.7, respectively.

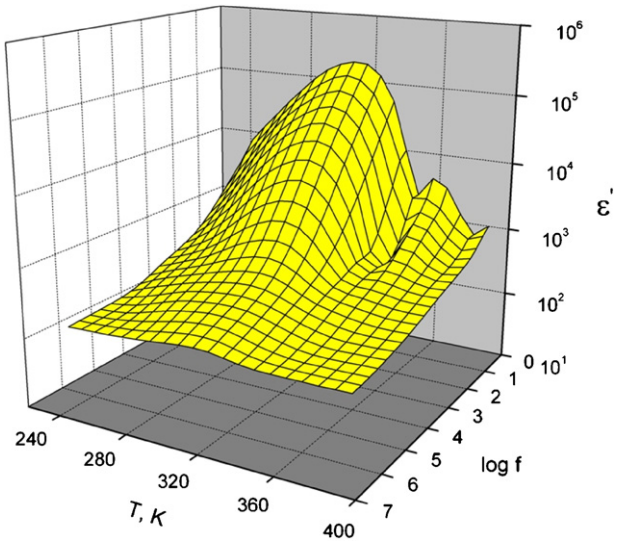

Fig. 5. Variation of the real part of dielectric constant (ε') with temperature and frequency.

Additionally, the measure of deflection from the Curie–Weiss law $\Delta T_m = T_{CW} - T_m$ has been found to be 35 K. Having a look at γ value, one can say that the sample is highly disordered. Broadening of phase transition is the result of disordered structures or compositional dispersion differences in the structure [26].

The dielectric constant decreases by increasing frequency at all temperatures, as it can be seen from the surface graph of the real part of dielectric constant. The frequency dependence of dielectric constant at low and particularly high temperatures is smooth. In fact, the dielectric constant is almost frequency-independent at high frequencies. However around DPT, the dielectric constant is rapidly decreasing at low frequencies. Dielectric behaviors of materials are usually explained by polarization phenomenon. For a solid state sample, each of electronic, ionic dipolar and surface charge polarizations contributes to the dielectric constant in their peculiar frequency ranges. Maxwell–Wagner (MW) model has been taken as a basis to characterize the rapid decrease of dielectric constant at sufficiently low frequencies [27]. According to this model, high dielectric constant is a result of polarization of surface charges. High polarization is due to non-homogeneous structure of the sample which is also supported by DPT. Thus the dielectric structure of the sample is composed of two regions, one of them is highly conductive, outnumbering and larger ferrite grains and the other is fairly poor conductive and smaller grain boundaries. While the grain boundaries are more effective at low frequencies, the grains are highly active at high frequencies [13]. Variation of conductivity in the interface between these regions results in an accumulation of charges in the grain boundary. Therefore this phenomenon involving a conductor and an insulator cannot be ignored at low frequencies. As frequency rises, the charges cannot follow applied external field and consequently cannot contribute to polarization [28]. So, the dielectric constant decreases rapidly at low frequencies. In this regard, a conductivity contribution term for the dielectric constant has to be considered at low frequencies.

Polarization mechanism of ferrites often occurs in a similar way to conductivity mechanism. An applied external electric field causes a polarization by displacing electrons with electronic exchange ($Fe^{2+} \leftrightarrow Fe^{3+} + e^-$). However, according to classical polarization mechanism, as frequency increases, the mobility of electrons in between Fe^{2+} and Fe^{3+} ion centers decreases. As a result, the dielectric constant becomes smaller after surface charge contribution loses its effect and gets eliminated [29,30].

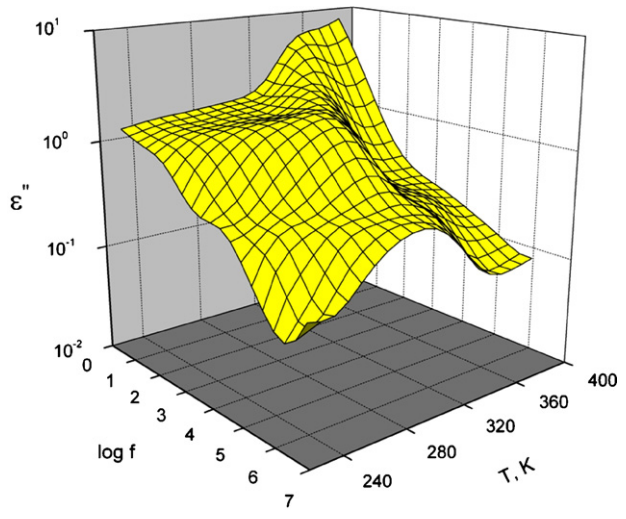

Fig. 6. Variation of the imaginary part of dielectric constant (ε'') with temperature and frequency.

As a comparison of literature, we have found greater values for dielectric constant compared with the $Ni_{0.5}Zn_{0.5}Fe_2O_4$ nanoparticles studied by various researchers [31–33].

3.5.2. Tangent loss

Temperature and frequency variation of the imaginary part of dielectric constant of the sample is shown in Fig. 6.

Tangent loss of the sample is strongly dependent on temperature and frequency as can be understood from very bumpy surface graph of the imaginary part (Fig. 6). However this behavior is dispersed in a wide range of temperature and the predicted DPT temperature of the real part can be clearly seen at high frequencies. Rapid decrease of the imaginary part at high temperatures reveals again the need for conductivity contribution just like the case of the real part. For the regions of tangent loss up to the anomaly at the phase transition temperature, it can be stated that the sample exhibits two dielectric relaxation phenomena corresponding to low and high frequency regions. Both of the relaxations shift to higher frequencies as the temperature rises, as a sign that they are thermally activated. Consequently, each of the relaxation times can be said to decrease with increasing temperature. Thus, the initial relaxation takes long-time, and the latter takes short-time to occur. However analyzing carefully, one can see that the short-time relaxation is not seen completely at high temperatures and that conductivity is dominant over long-time relaxation. Considering the frequencies at which relaxations occur, the one happening at lower frequency is based on surface charge relaxation and the one occurring at higher frequency is based on the fact that the magnitude of applied external field frequency and the hopping frequency of exchange electrons between Fe^{2+} and Fe^{3+} are almost equal to each other [34].

Tangent loss is dependent on the real and imaginary parts by ($\varepsilon'' = \varepsilon' \tan\delta$). It is technologically important to appreciate the cases where $\tan\delta$ has large values. Again comparing tangent loss values, tangent loss values of 1.9 and 0.26 obtained at 10 kHz and 1 MHz measurements which are larger than those found in other Ni–Zn ferrites [31–33]. Therefore, considering the effects of temperature on tangent loss, the value of 1 around the room temperature and relatively higher values gain importance in terms of technological applications. Up to this end, making use of present NPs in temperature induced gene expression and destruction of ill-cells without damaging healthy cells by targeting NPs at tumors should be discussed [35]. Furthermore, the sample with its low dielectric loss possesses potential in terms of high frequency applications.

3.5.3. Argand diagram

The dependence of the imaginary part on the real part of the dielectric constant is shown in Fig. 7.

Together with small circular curve at higher frequencies and large curve at lower frequencies, the graphs look like each other. The argent diagram reveals two sequential frequency-induced relaxation mechanisms as predicted clearly by tangent loss. The large curve corresponds to the long-time relaxation and the small curve indicates the short-time relaxation. Sharp incidence of the large curve with the low frequency is again represented by the conductivity contribution. The centers of curves being below the real axis and symmetric behavior of frequency dependence of the tangent loss related imaginary part around the peak can be appropriately explained within the frame of Cole–Cole model. The two relaxations can be theoretically explained by adding the conductivity term to this model. In this context, the frequency dependence of the real and the imaginary parts of dielectric constant are as follows

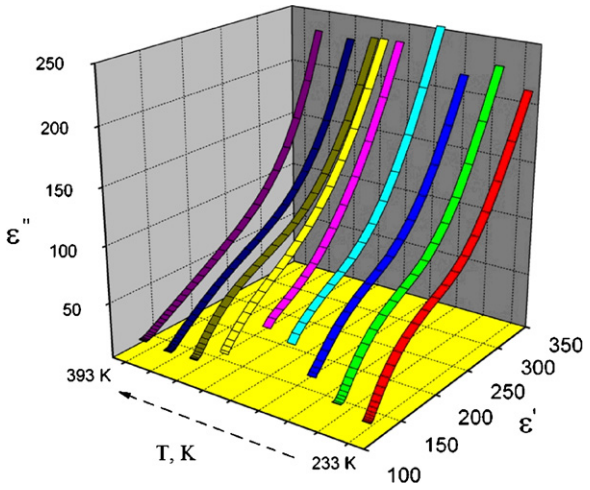

Fig. 7. Variation of the imaginary part of dielectric constant with its real part at some selected temperatures.

[36].

$$\varepsilon'(w,T) = \varepsilon_\infty + \sum_{n=1}^{2} \frac{\Delta\varepsilon_n \cos\varphi_n}{[1 + 2(w\tau_n)^{\alpha_n} \sin\pi(1-\alpha_n)/2 + (w\tau_n)^{2\alpha_n}]} + \frac{\sigma_o}{\varepsilon_o w^s} \cos\frac{\pi s}{2} \quad (2)$$

$$\varepsilon''(w,T) = \sum_{n=1}^{2} \frac{\Delta\varepsilon_n \sin\varphi_n}{[1 + 2(w\tau_n)^{\alpha_n} \sin\pi(1-\alpha_n)/2 + (w\tau_n)^{2\alpha_n}]} + \frac{\sigma_o}{\varepsilon_o w^s} \sin\frac{\pi s}{2} \quad (3)$$

Here, φ_n is identified as the following,

$$\varphi_n = \arctan\left[\frac{(w\tau_n)^{\alpha_n} \cos\pi(1-\alpha_n)/2}{1 + (w\tau_n)^{\alpha_n} \sin\pi(1-\alpha_n)/2}\right] \quad (4)$$

Here, $\Delta\varepsilon$ stands for dielectric strength, w denotes angular frequency, τ is the relaxation time, α is the relaxation distribution parameter, σ_o represents the DC conductivity and s is the power parameter of conductivity. The dielectric strength of long-time relaxation at low frequencies is fairly greater than that of short-time as can be seen in the circular curves. This clearly reveals the effect of surface charges. Analyzing high frequency relaxations, as temperature rises; the dielectric strength initially decreases and later increases. The variance of relaxation times obtained after fitting them is plotted in Fig. 8.

Temperature variation of this characteristic parameter is represented by $\tau(T) = \tau_o \exp(-(E_a/k_B T))$ and according to this equation; the activation energies have been calculated to be 0.13 eV for the long-time relaxation, and 0.22 eV for the short-time relaxation.

3.5.4. Conductivity

Conductivity response of the sample to the applied AC field at some selected temperatures is given in Fig. 9.

Again by looking at Fig. 9, one can say that the sample has strong temperature and frequency dependence. There exists an anomaly around 305 K in the temperature dependence of conductivity just as seen in other electrical properties. An increase in conductivity with increasing frequency at all temperatures is a universal result. This behavior is particularly composed of two parts. The first of them is the DC conductivity part that represents the band conductivity and is characterized by plateaus behavior seen at low frequencies with temperatures above 380 K. The second part is the

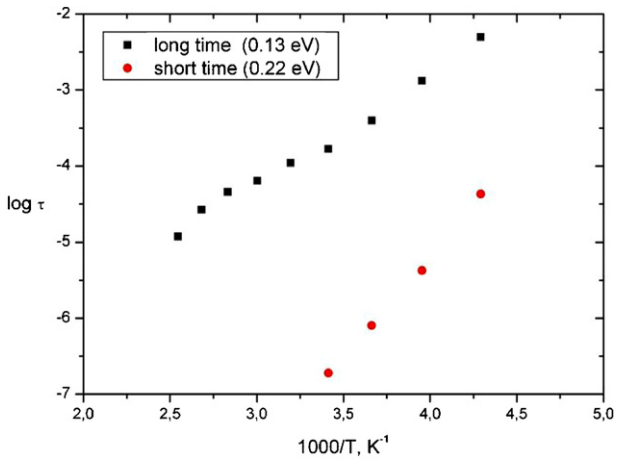

Fig. 8. Temperature variation of relaxation times.

AC conductivity which tends to rapidly increase at high frequencies. The frequency dependent conductivity is formulated as the sum of these two parts. This behavior can be represented by Jonscher's power law as follows [37].

$$\sigma(w) = \sigma_o + Bw^{s(T)} \quad (5)$$

In this expression, w is the angular frequency given by ($w = 2\pi f$), B is a temperature-dependent constant and the index s is the previously mentioned power parameter having a value less than 1. This characteristic parameter is obtained from the slope of the curve in the log–log graph of conductivity vs. frequency. For a system under investigation, temperature variation of the value of s gives information about the conductivity mechanism of that system [38].

For spinel structures, the power parameter generally decreases with increase in temperature and their conductivity behavior is explained by Correlated Barrier Hopping (CBH) model in some studies [39]. Whereas there are also a few studies in which small polaron hopping [40] and quantum mechanical tunneling [41] types of conductivity are reported to take place. Here, it is clear that as the temperature rises, this parameter decreases up until a bottom dip and then increases after that bottom dip as seen in Fig. 10. Thus, for the measured temperature range, the conductivity mechanism of the sample can be stated to be overlapping large polaron tunneling (OLPT) [38,42].

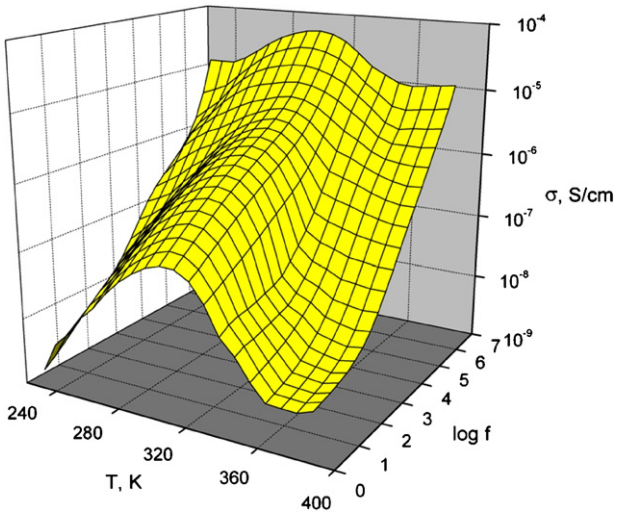

Fig. 9. Variation of conductivity with temperature and frequency.

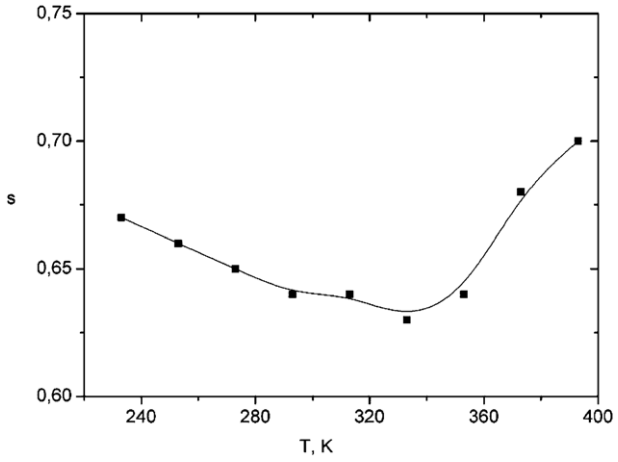

Fig. 10. Temperature variation of the power parameter (s) of conductivity.

This is a mechanism which envisions that polaron energy can be derived from the polarization variations in the lattice [43]. According to OLPT type of conductivity, since Coulomb interaction occurs in long range, potentials of neighboring sites are in a state of overlapping on one another. This state also makes the overlapping of polaron cloud which should not be ignored. Formation of polarons can generally be observed in nanosystems containing ferrites. This formation is caused by having the defect levels at nanometer scale [38]. According to the model, solely frequency dependent second part of Eq. (5) and the power parameter are identified as follows [44],

$$\sigma(w) = \frac{\pi^4}{12} e^2 (k_B T)^2 [N(E_F)]^2 \frac{w {R_w}^4}{[2\alpha k_B T + ((r_p W_{Ho})/{R_w}^2)]} \quad (6)$$

$$s = 1 - \frac{8\alpha R_w + (6 r_p W_{Ho}/R_w k_B T)}{(2\alpha R_w + (r_p W_{Ho}/R_w k_b T))^2} \quad (7)$$

In Eqs. (6) and (7), R_w represents the optimum tunneling distance for the polaron and r_p denotes the polaron radius. For the small values of polaron radius, the value of s decays to a minimum at a possible temperature and then increases as temperature gets higher and higher [45]. The term α stands for the decay constant of the polaron wave function, W_{Ho} represents the polaron hopping energy and the rest are the classical parameters well-known in the literature.

To make another comparison with literature, the conductivity values of 0.334 μS/m, 0.467 μS/m and 2.75 μS/m obtained at 1 kHz, 10 kHz and 1 MHz, respectively are each greater than calculated conductivity values of 0.109 μS/m, 0.298 μS/m and 1.85 μS/m which belong to undoped $Ni_{0.5}Zn_{0.5}Fe_2O_4$ ferrite examined by Nasir et al. [31]. So it can be asserted that Cr doping increases conductivity of Ni–Zn ferrites. They have also found some dielectric constant values of Cr doped Ni–Zn nano ferrites. For their sample Cr-5 whose chemical formula is the same as our sample they found dielectric constant as 17.17 at 10 kHz and 13.79 at 1 MHz measurements done at room temperature. The corresponding dielectric constant values of our sample are 44.97 and 17.37, respectively which indicates that our sample possess a higher dielectric constant which may be dependent on structure and size of the NPs and effect of PEG coating. It can also arise from synthesis condition and oxygen deficiency on the surface of the NPs [46].

4. Conclusions

In this study, chromium substituted Nickel–Zinc ferrite NPs of $Ni_{0.5}Zn_{0.5}Cr_{0.5}Fe_{1.5}O_4$ have been synthesized successfully by using surfactant-assisted hydrothermal technique. The structure and the elemental composition of the sample were confirmed by FT-IR, XRD, FE-SEM and EDX. The crystallite size of the product was found as 34 nm by applying Debye–Scherrer equation on the XRD pattern.

An anomaly exhibited by electrical properties around 305 K reveals that the sample shows a phase transition characterized by DPT around this temperature. The giant dielectric constant at this temperature has been explained by the MW model by taking surface charges into account. The dielectric behavior has been accounted for the presence of two different modified relaxation mechanisms and the additional conductivity contribution. It has been determined for the sample that there are two kinds of relaxations; short-time relaxation and long-time relaxation with activation energies of 0.22 eV and 0.13 eV, respectively. The electrical conductivity of the system has been theoretically supported by the OLPT model.

Experimental results with the loss factor having high values at appropriate temperatures give the sample importance in terms of technologic low-frequency applications. Likewise, a potential in terms of high-frequency applications may also be mentioned due to the low dielectric losses. The sample should also be given attention for the semiconducting properties it exhibits. The giant dielectric constant of the sample should be noted too. All in all, technological applicability of the present ferrite system should be assessed by carrying out further studies.

Acknowledgements

This research was supported by Fatih University under grant no: P50021002-G.

Appendix A. Supplementary data

Supplementary data associated with this article can be found, in the online version, at doi:10.1016/j.jallcom.2011.07.063.

References

[1] K. Mandal, S.P. Mandal, P. Agudo, M. Pal, Appl. Surf. Sci. 182 (2001) 386–389.
[2] H. Yang, L. Shen, L. Zhao, Mater. Lett. 57 (2003) 2455–2459.
[3] H. Yang, D. Wang, Z. Wang, M. Zhao, M. Li, L. Wang, Mater. Chem. Phys. 48 (1997) 212–215.
[4] H. Yang, F. Wu, L. Song, M. Zhao, J. Wang, H. Luo, J. Magn. Magn. Mater. 134 (1994) 134–136.
[5] S.K. Pradhan, S. Bid, M. Gateshki, V. Petkov, Mater. Chem. Phys. 93 (2005) 224–230.
[6] V. Sepelak, K.D. Becker, J. Mater. Synth. Process 8 (2000) 155–166.
[7] M. Sertkol, Y. Köseoğlu, A. Baykal, H. Kavas, A.C. Başaran, J. Magn. Magn. Mater. 321 (2009) 157–162.
[8] M. Sertkol, Y. Köseoğlu, A. Baykal, H. Kavas, A. Bozkurt, M.S. Toprak, J. Alloys Compd. 486 (2009) 325–329.
[9] H. Kavas, A. Baykal, M.S. Toprak, Y. Köseoğlu, M. Sertkol, B. Aktaş, J. Alloys Compd. 479 (2009) 49–55.
[10] M. Sertkol, Y. Köseoğlu, A. Baykal, H. Kavas, M.S. Toprak, J. Magn. Magn. Mater. 322 (2010) 866–871.
[11] H. Igarashi, K. Okazaki, J. Am. Ceram. Soc. 60 (1977) 51–54.
[12] T. Abraham, Am. Ceram. Soc. Bull. 73 (1994) 62–65.
[13] A.M. Abdeen, J. Magn. Magn. Mater. 192 (1999) 121–129.
[14] P. Yadoji, R. Peelamedu, D. Agrawal, R. Roy, Mater. Sci. Eng., B 98 (2003) 269–278.
[15] B.P. Rao, K.H. Rao, T.V. Rao, A. Paduraru, O.F. Caltun, J. Optoelectron Adv. Mater. 7 (2005) 701–704.
[16] A. Narayanasamy, N. Sivakumar, Bull. Mater. Sci. 31 (2005) 373–380.
[17] M. Ajmal, A. Maqsood, Mater. Lett. 62 (2008) 2077–2080.
[18] S. Deka, P.A. Joy, J. Am. Ceram. Soc. 90 (2007) 1494–1499.
[19] J. Azadmanjiri, Mater. Chem. Phys. 109 (2008) 109–112.
[20] I.H. Gul, W. Ahmed, A. Maqsood, J. Magn. Magn. Mater. 320 (2008) 270–275.
[21] B.P. Rao, K.H. Rao, J. Mater. Sci. 32 (1997) 6049–6054.
[22] A.D. Sheikh, V.L. Mathe, J. Mater. Sci. 43 (2008) 2018–2025.
[23] J. Smith, H.P.J. Wijn, Ferrites, Wiley, New York, 1959.
[24] A.A. Sattar, H.M. El-Sayed, K.M. El-Shokrofy, M.M. El-Tabey, J. Mater. Eng. Perform. 14 (2005) 99–103.
[25] S.K. Rout, E. Sinha, S. Panigrahi, Mater. Chem. Phys. 101 (2007) 428–432.

[26] S.K. Rout, E. Sinha, S. Panigrahi, J. Bera, T.P. Sinha, J. Phys. Chem. Solid 67 (2006) 2257–2262.
[27] M. Ajmal, A. Maqsood, Mater. Sci. Eng., B 139 (2007) 164–170.
[28] M.A. Elkestawy, S.A. Kader, M.A. Amer, Phys. B 405 (2010) 619–624.
[29] S.M. Patange, S.E. Shirsath, K.S. Lohar, S.S. Jadhav, N. Kulkarni, K.M. Jadhav, Phys. B 406 (2011) 663–668.
[30] A.M.M. Farea, S. Kumar, K.M. Batoo, A. Yousef, C.G. Lee, Alimuddin, J. Alloys Compd. 464 (2008) 361–369.
[31] S. Nasir, G. Asghar, M.A. Malik, M. Anis-ur-Rehman, J. Sol–Gel Sci. Technol. 59 (2011) 111–116.
[32] K. Bhattacharjee, C.K. Ghosh, M.K. Mitra, G.C. Das, S. Mukherjee, K.K. Chattopadhyay, J. Nanopart. Res. 13 (2011) 739–750.
[33] M. Atif, M. Nadeem, R. Grossinger, R. Sato Turtelli, J. Alloys Comp. 509 (2011) 5720–5724.
[34] D. Ravinder, A.C. Reddy, Mater. Lett. 57 (2003) 2855–2860.
[35] M.A. Elkestawy, J. Alloys Compd. 492 (2010) 616–620.
[36] T. Raissi, N. Ramdani, L. Ibos, Y. Candau, Proceedings of the 5th International Conference on Inverse Problems in Engineering: Theory and Practice, vol. 3, 11–15 July 2005, Leeds University Press, Cambridge, UK, 2005, R01, ISBN: 085316242.
[37] A.K. Jonscher, Nature 267 (1977) 673–679.
[38] E.V. Gopalan, K.A. Malini, S. Saravanan, D.S. Kumar, Y. Yoshida, M.R. Anantharaman, J. Phys. D: Appl. Phys. 41 (2008) 185005.
[39] M.K. Fayek, M.F. Mostafa, F. Sayedahmed, S.S. Ata-Allah, M. Kaiser, J. Magn. Magn. Mater. 210 (2000) 189–195.
[40] Y.C. Chung, H.I. Yoo, J. Mater. Res. 16 (2001) 774–777.
[41] A.M.A.E. Ata, S.M. Attia, T.M. Meaz, Solid State Sci. 6 (2004) 61–69.
[42] S.A. Mansour, I.S. Yahia, G.B. Sakr, Solid State Commun. 150 (2010) 1386–1391.
[43] A.R. Long, Adv. Phys. 31 (1982) 553–637.
[44] Aloka Ghosh, S. Bhattacharya, D.P. Bhattacharya, A. Ghosh, J. Phys.: Condens. Matter 20 (2008) 035203.
[45] W.H. Jung, Phys. B 403 (2008) 636–638.
[46] S. Nasir, M. Anis-ur-Rehman, M.A. Malik, Phys. Scr. 83 (2011) 025602.